

# Transient Co-Simulation of Electromagnetic Emissions caused by a SiC Traction Inverter

P. Hillenbrand\*, M. Beltle, S. Tenbohlen

Institute of Power Transmission and  
High Voltage Technology  
University of Stuttgart, Germany

\*philipp.hillenbrand@ieh.uni-stuttgart.de

Jan Hansen

Automotive Electronics  
Robert Bosch GmbH  
Schwieberdingen, Germany  
jan.hansen@de.bosch.com

**Abstract**— We present EMI simulations of a silicon carbide MOSFET traction inverter. The simulations are based on a transient circuit simulation and frequency domain simulations of different 3D geometry models. In a first step, an equivalent circuit is derived from parts of the geometry model and combined with an analytical model of the MOSFETs and an equivalent circuit model of the DC link capacitor. The results from the time domain simulation are used as input data for a frequency domain simulation in a second step. This part of the simulation is based on geometry models of the complete CISPR25 test setup including one monopole and one biconical antenna. The combination of both simulations can reproduce the conducted and radiated emissions of the inverter up to 110 MHz even if a filter network is added to the DC side of the inverter.

**Keywords**—traction inverter; EMI simulation; CISPR25; transient-co simulation, CST Microwave Studio

## I. INTRODUCTION AND TEST SETUP

New wide-bandgap semiconductor materials offer promising possibilities and lead to new challenges in the field of traction inverters in electric vehicles. The positive aspects: Inverters based on SiC or GaN MOSFETs can increase the efficiency of an electric drive train especially during partial load conditions [1]. Even more remarkable is the optimization related to the volume of the inverter. Using SiC MOSFETs as semiconductor switches allows higher battery voltages and lower semiconductor power losses at the same time. A smaller capacity and volume of the DC link capacitor and the semiconductors is needed because the reduced switching losses enable higher switching frequencies. In addition, the operating temperature of SiC MOSFETs can be much higher compared to silicon-based semiconductors which lead to a decreased size of the inverter's heat-sink. The combination of these effects can reduce the volume of the inverter by a considerable proportion [2]. The negative aspects: Higher battery voltages, higher switching frequencies and faster switching times increase electromagnetic interferences. A simple example shows the effect of changing these parameters. Therefore the common-mode equivalent circuit presented in [3] is used to simulate the disturbance voltage at the Line Impedance Stabilization Network (LISN) of a conventional Si-IGBT inverter compared to a new designed SiC inverter. Fig. 1 shows the result of the simulation. A change of system parameters in the presented scenario leads to an increased disturbance voltage by 18 dB in CISPR Band B

and by 33 dB in CISPR Band C, see Fig. 1. Starting from the premise that car manufacturers intend to use unshielded battery-cables in future electric vehicles will require large EMI filters which will contribute a considerable proportion of the inverter's total volume. This circumstance requests the integration of EMI simulations in the optimization process of the inverter. Here, the essential precondition is a fast and precise simulation of conducted and radiated emissions of the inverter including all necessary filter elements.

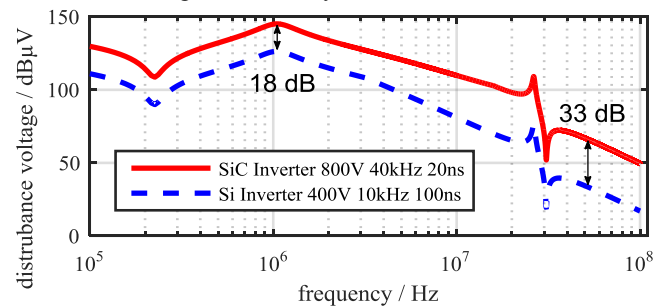


Fig. 1. Influence of drive-drain parameters on the EMI of the inverter. Higher battery voltages, switching-frequency and switching-time cause higher EMI.

In order to fulfill this goal, this contribution uses the test setup presented in Fig. 2 to investigate EMI simulation techniques. The setup is similar to the case defined in CISPR25 and consists of two LISNs, the inverter, and a loadbox. All components are mounted on a conductive table representing the car body and connected to each other with unshielded cables.

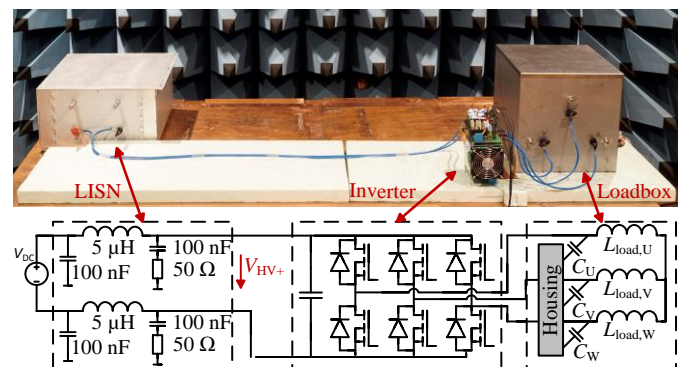


Fig. 2. Picture and simplified equivalent circuit of the test setup consisting of two LISNs, an inverter based on SCT2080ke SiC MOSFETs and a 3-load.

The inverter is based on SCT2080ke SiC-MOSFETs produced by Rohm™, connected to each other in three half-bridges. The DC link capacitor with a total capacity of 17.2  $\mu\text{F}$  is built up with electrolytic capacitors and ceramic capacitors placed on a PCB very close to the switches. In order to minimize the influence of the control electronics, battery supplied gate-units with optical fiber-transmitted control signals are used at the top of the main PCB. A control algorithm based on a sine-triangle comparison with a modulation degree of 30 % and a carrier signal frequency of  $f_{\text{PWM}} = 20.2 \text{ kHz}$  is used to control the inverter (blanking time  $t_b = 800 \text{ ns}$ ). For all measurements and simulations the DC voltage is set to  $V_{\text{DC}} = 180 \text{ V}$ .

The electromagnetic emissions caused by the inverter are characterized in the test setup by disturbance voltages. Conducted emissions are represented by the voltage  $V_{\text{HV}+}$  at the LISN and radiated emissions by antenna voltages (described in Sect. IV). The EMC limits of these voltages are usually defined by the vehicle manufacturer in the frequency domain and verified with an EMI test receiver. For simplicity reasons, this investigation neglects the detector circuits of the test receiver and uses oscilloscope measurements which are transformed into frequency domain using a FFT algorithm. The overall goal of this study is a precise simulation of all necessary disturbance voltages without the existence of a prototype of the inverter.

## II. GENERAL SIMULATION APPROACH

Concerning conducted emissions, a frequency domain simulation based on a 3D geometry model of a CISPR25 component test setup is able to reproduce the disturbance voltage at the LISN caused by a DCDC converter [4]. However, [4] uses measured voltages of the MOSFETs during the operation of the device as input parameters. In this paper the necessary measurements are replaced by a transient simulation. Furthermore the device under test is extended to a three-phase traction inverter and the new simulation considers now radiated emissions, as well.

The time domain simulation of the inverter is based on the geometry model pictured in Fig. 3. The model is created in CST Microwave Studio™ and computed to a multiport system including all elements of the test setup. The solution of the model describes all necessary parasitic elements of the inverter in form of a linear and time independent (LTI) n-port system. However, this frequency domain solution cannot be used directly in a time domain simulation. First, a time domain equivalent needs to be found.

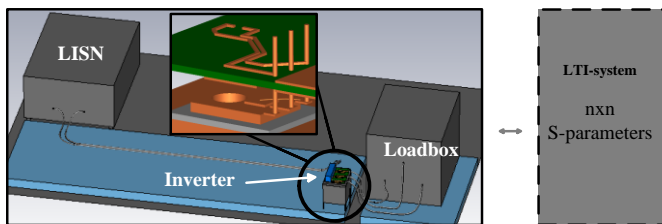


Fig. 3. AC simulation model for the LTI part of the test setup

If this solution is found, the disturbance voltage e.g. at the LISN can either be gained from the transient simulation directly or with the method described in [4]. Therefore, the

simulated drain-source voltages of all MOSFETs are transformed into frequency domain and used as excitation in the frequency domain simulation in the form of ideal voltage sources, according to the principle illustrated in Fig. 4.

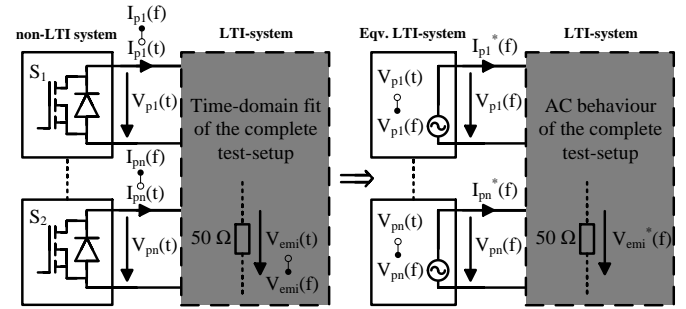


Fig. 4. Basic principle of a transient co-simulation. The drain-source voltages of the MOSFETs are transformed to frequency domain and used as excitation in the AC model in the form of ideal voltage sources.

The complexity of the time domain fit mostly depends on the complexity of the geometry. Concerning the dimensions of the CISPR25 test setup, transient circuit simulations of the entire geometry tend to be time consuming and can cause convergence problems. In this case, using the drain-source voltages as excitation in a frequency domain simulation can offer the benefit of a simpler and faster transient simulation. For this method, the time domain simulation needs to cover only elements that encounter the shape of the drain-source voltage which is only a small part of the test setup. To identify the required elements, we measure the drain-source voltage during one switch-on, and one switch-off event of a low-side MOSFET in different configurations of the test setup. Fig. 5 shows the results of this sensitivity analysis. The reference curves are recorded in the CISPR25 test setup. Afterwards, the conductive table of the test setup is removed and the DC supply is connected directly to the inverter with a short cable instead of the LISN. In a third measurement, the filter introduced in Sect. V is added to the DC side of the inverter.

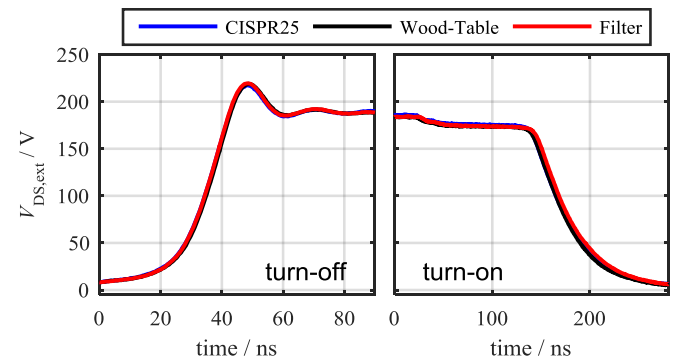


Fig. 5. Influence of the conductive table and the LISN on the shape of the drain-source voltage during switch-on and switch-off of a low-side MOSFET.

Fig. 5 shows no visible deviation between the drain-source voltages measured in the three different test setups. This allows the assumption, that a successful simulation of all drain-source voltages of the MOSFETs requires only the elements of the commutation-cell and the differential impedances between the motor-cables and the loadbox. Additional filter elements need to be included to the time domain simulation only if they change these impedances. In

general, this can be neglected for filter elements at the DC side of the inverter due to the very low inductance of the DC link capacitor. The new simulation approach is illustrated in Fig. 6. Here, the drain-source voltages are simulated in time domain with a simple equivalent circuit and used as excitations in the subsequent frequency domain simulation. The equivalent circuit needs to be valid from DC up to the maximum frequency but the geometry is much simpler and enables the creation of a physically interpretable equivalent circuit.

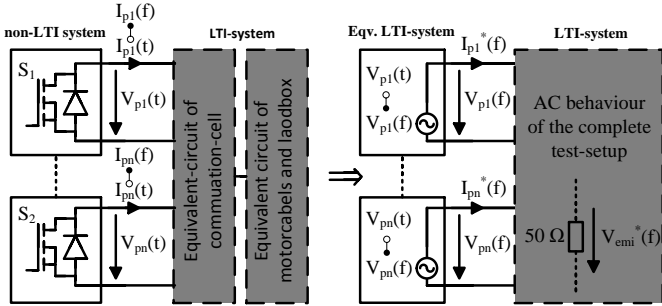


Fig. 6. Simplification of transient simulation by reducing the LTI-system to the relevant parts of the commutation-cell of the inverter.

The following sections investigate the above-described approach. Sect. III explains how the equivalent circuit is derived from the 3D-geometry model of the commutation-cell and describes the used models of the MOSFETs and the DC link capacitors. The results are compared in time domain with oscilloscope measurements of the real test setup. Sect. IV uses these results as excitations in different 3D geometry frequency domain models to obtain the conducted and radiated emissions of the inverter. Finally, Sect. V includes a filter network at the DC side of the inverter in the test setup and the simulation and compares the EMI results.

### III. TRANSIENT SIMULATION OF THE COMMUTATION-CELL

#### A. Simplified Transient Simulation

To simplify the creation of the necessary equivalent circuit as much as possible, the commutation-cell is divided into three identical half-bridges shown in Fig. 7.

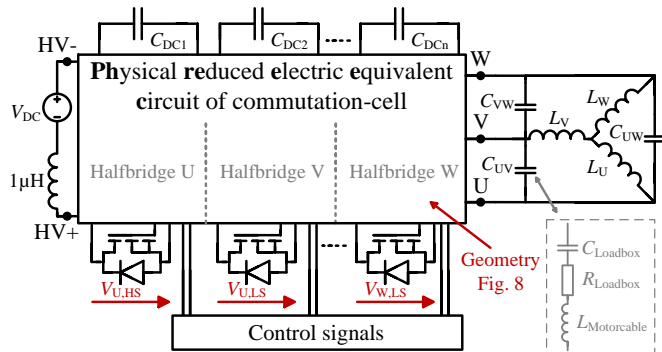


Fig. 7. Structure of simplified transient simulation of the commutation-cell.

One DC voltage source supplies the inverter decoupled with a single inductor. The differential impedances between U, V and W are reproduced by the inductors  $L_U$ ,  $L_V$  and  $L_W$  with a value between 128 and 131  $\mu\text{H}$  connected to a star and the capacitors  $C_{UV}$ ,  $C_{VW}$  and  $C_{UW}$  with a capacitive value between

1.98 and 2.05 nF connected to a triangle. Each capacitor is modeled as a series connection of one capacitor, one resistor and one inductor. These elements fit very well to the impedance between U, V and W if short motor cables are used.

The circuit elements inside the three half bridges are calculated from the geometry model. Therefore Fig. 8 shows the 3D model of one half-bridge with 21 points defined on the surface of the structure. These points are defined as circuit nodes of the resulting equivalent circuit. Different methods can be used to compute the elements between these points. This paper uses the method described in [4] and obtains partial inductances between galvanic connected nodes and parasitic capacitances between isolated nodes. As described in [4] the capacitances are calculated with an electrostatic solver and the inductances are computed from the eigenmode solution of the geometry model using the algorithm described in [5].

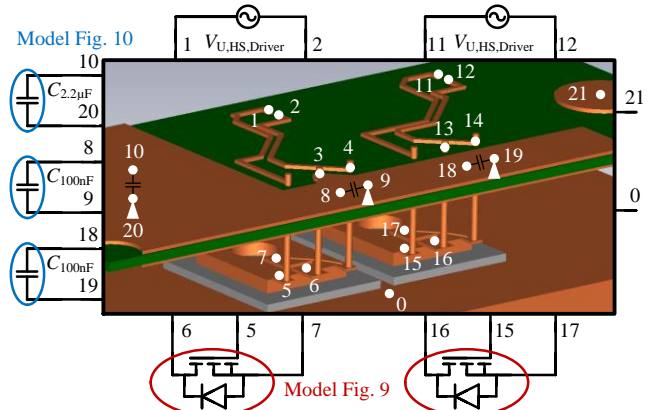


Fig. 8. Computing necessary parasitic elements from the geometry model.

Alternatively, a linear macro model [8] or a partial electric equivalent circuit (PEEC) [9] can be created. Tools for both methods are commercially available, but the significant advantage of the method presented here is the creation of a physically interpretable equivalent circuit. The presented solution consists only of resistors, capacitors and coupled inductors which are connected to a comprehensible and stable equivalent circuit.

To complete the time domain simulation of the commutation-cell, models of the DC link capacitors, the MOSFETs and the control voltages of the gate drivers are attached to the equivalent circuit. The gate driver voltages are calculated according to [3] and the capacitor and MOSFET models are described below.

#### B. MOSFET Model

Fig. 9 shows the used MOSFET model consisting of two voltage-dependent chip capacitances  $C_{GD}$  &  $C_{DS}$ , one internal gate resistance  $R_G$ , a fixed gate-source capacitance  $C_{GS}$  and two current sources  $I_{DS}$  &  $I_{SD}$  representing the IV-curves of the MOSFET and the body-diode. The input data is extracted from the datasheet of the MOSFET. Voltage dependent current sources are directly accessible in Spice and can be defined as a function of node voltages or currents between nodes. It is essential to use continuous and differentiable functions for these sources in order to avoid convergence problems. Voltage dependent capacitances are not directly accessible in Spice.

Therefore, a capacitor of  $C_1 = 1 \text{ pF}$  is used in combination with one voltage dependent current source  $I_C$  connected in parallel. The current source amplifies the current through  $C_1$ , thereby  $C_{DS}$  appears to be dependent on  $V_{DS}$ . Ref. [6] describes the implementation of the model in detail and shows the relevant parameters for the EMI simulation of the inverter.

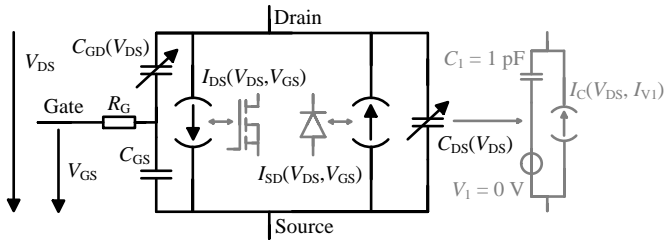


Fig. 9. Circuit elements of used MOSFET model.

### C. Equivalent Circuit of DC Link Capacitor

To model the frequency dependent behavior of the DC link capacitor, the equivalent circuit in Fig. 10 is used. The circuit models the imaginary and real part of the DC link capacitor impedance precisely.

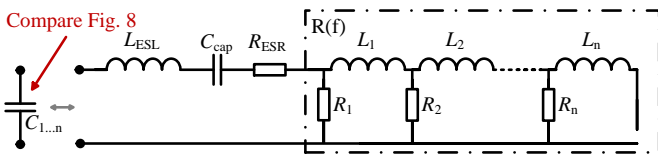


Fig. 10. Equivalent circuit used for DC link capacitors.

For the parametrization the elements  $L_{ESL}$ ,  $C_{cap}$  and  $R_{ESR}$  are calculated directly from measurements of the DC link capacitor by using the magnitude of the impedance.  $L_1$  to  $L_n$  and  $R_1$  to  $R_n$  are fitted values to consider the frequency dependent losses inside the capacitor.

### D. Time Domain Simulation Results

The time domain simulation described in Sect. II A-C is implemented in LT-Spice V2.3 and solved with the alternate solver option. Using a maximum time-step of 2 ns and a stop time of 1 ms, computation times are approximately 6 min. Fig. 11 shows the result of the simulation for one load-cycle.

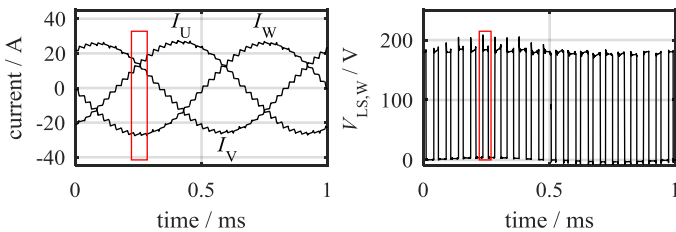


Fig. 11. Time domain simulation result of one load cycle. Left: Load currents of 3-load. Right:  $V_{DS}$  of the low-side MOSFET (halfbridge W).

To compare the simulation results with the measurements the focus lies on one turn-off and one turn-on event, marked in red in Fig. 11. It is impossible to measure the drain-source voltage  $V_{DS}$  of the semiconductor chip in the real test setup because the chip is hidden inside the package. Therefore, Fig. 12 compares the drain-source voltage of the low-side MOSFET of half-bridge W at the MOSFET pins between the points 13 and 14 marked in Fig. 8.

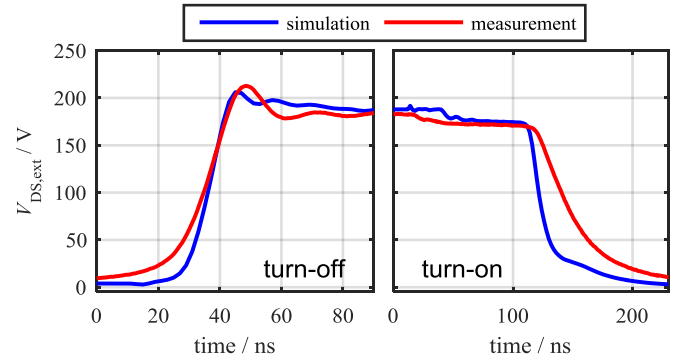


Fig. 12. Comparison of the measured and simulated drain-source voltage of one low-side MOSFET (halfbridge W) during switch-on and switch-off.

For both the turn-on and the turn-off event, the simulation is able to reproduce the shape of the voltage curves, but in the simulation the rise-time and the fall-time are shorter than the measured ones. This phenomenon is investigated in [6] and leads back to underestimated semiconductor capacitances. Especially the voltage dependent gate-drain capacitance  $C_{GD}$  depends highly on the gate-source voltage  $V_{GS}$ . During switching,  $C_{GD}$  can be increased by a factor of 2 to 3 compared to the value measured in a static off-state of the MOSFET [7].

In the next step, the transient simulation results of  $V_{DS}$  (at the semiconductor chip) of all MOSFETs are used as excitations in a frequency domain simulation. Therefore the voltages of a full load-cycle (1 ms) are transformed into frequency domain using a FFT algorithm and imported as frequency dependent ideal voltage sources in the following frequency domain simulations.

## IV. SIMULATION SETTINGS OF THE COMPONENT TEST

Two full 3D computer models are created using the CST Studio Suite in order to simulate conducted and radiated emissions. One model contains a monopole (Fig 13a), the second a biconical antenna in horizontal orientation (Fig 13b).

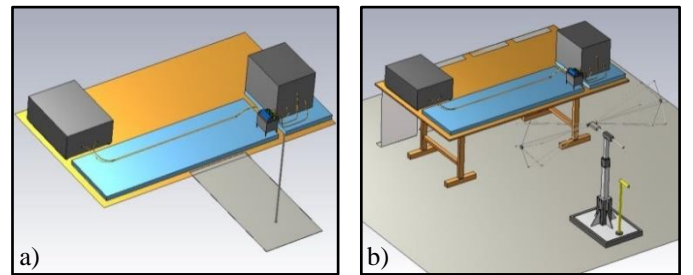


Fig. 13. Geometry models used for the simulation of radiated emission. a) Monopole antenna VAMP 9234. b) Biconical antenna VHBC 9133.

Both models are constructed according to the CISPR25 standard. For sufficient accuracy, a suitable 3D model of present size characterizes all relevant parts of the geometry, but it cannot model all details of its electronics. For that reason, the electronic parts of the LISNs and the load-box are characterized by S-parameter measurements. In the 3D simulation model, the metallic outer surfaces of the containers with the LISNs and the load-box are modelled, and ports connect those boxes with the stubs of the wires which are routed to them. The identical procedure is done for the capacitors of the commutation-cell and the BALUN of the

antennas where in the 3D model ports replace any electronics details. Finally, 6 ports are located at the positions of the switches. A large geometric model results with a total number of 37 ports in case of the monopole antenna and 38 ports in case of the biconical antenna.

Both models are discretized with a tetrahedral mesh, resulting in 170k mesh-cells for the monopole antenna ( $f_{\max} = 110$  MHz) and 350k mesh-cells for the model with the biconical antenna ( $f_{\max} = 200$  MHz). Using the fast reduced order model solver, computation times are 14 and 26 min, yielding a multiport network description of the 3D model.

All capacitors are characterized by 1-port network analyzer measurements, the box with the two LISNs is measured as 4-port (two lines in and two measurement ports), and the load-box as a 3-port. The antennas are measured as shown in Fig. 14. The monopole antenna rod is detached from the feeding network, so that the electrical properties of the feeding network can be characterized by a 2-port network analyzer measurement between the antenna feeding point and the output to the rod. In case of the biconical antenna, both wings are detached and the network analyzer measurement describes the antenna's BALUN as a 3-port between feeding connector and antenna wings.

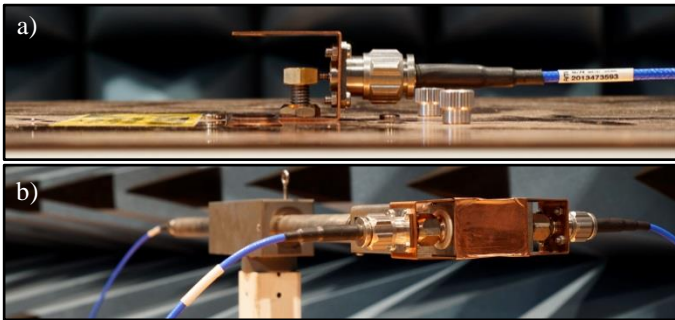


Fig. 14. Antenna characterization used for the simulation of radiated emission. a) Monopole antenna VAMP 9234. b) Biconical antenna VHBC 9133.

Finally, at each pin the computed multiport network is assembled with the measured S parameters of the respective termination. The six pins at the locations of the switches remain as excitation pins of the model. The observation port is either at one of the LISNs in case of a conducted emission measurements, or at the antenna foot in case of the radiated measurements. In each case, we basically obtain a 7-port network description, where six of the ports are used for excitation with the ideal voltage sources gained from the time domain simulation of the commutation-cell and the remaining port for observation of the frequency domain simulation result. The results of all frequency domain simulation are summarized in Sect. V.

## V. IMPLEMENTATION OF FILTER ELEMENTS

The filter shown in Fig. 15 was created in order to show the ability of the model to include complex filter networks. The filter is designed for demonstration purpose only and not optimized to fulfill any given EMC limit. It consists of two copper-bars routed through a magnetic core of nano-permeable material and a pair of  $C_Y$  capacitors on each side of the ring. One pair of capacitors is chosen to 3.3  $\mu$ F capacitance, and the other one to 680 nF. Additionally, a

resistor of 1 k $\Omega$  is added in series to each of the 680 nF capacitors to attenuate the filter resonance. The magnetic properties of the nano-permeable material are characterized by its complex permeability over frequency.

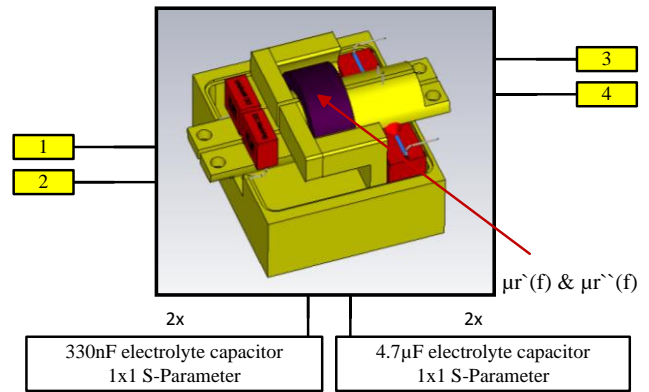


Fig. 15. Geometry model of investigated filter consisting of one nano-permeable ring and two different types of  $C_Y$ -capacitors.

In the simulation the geometric shape of the capacitors is modeled as a perfect electric conductive box which is sliced into two half sections. Both sections are connected by a port which is terminated in the subsequent network simulation by a measured 1-port characterization of the respective capacitor. Because the measurement includes the inductive behavior of the capacitor beyond its resonance, which is also modeled in 3D, a negative partial inductance of -20 nH is applied in the simulation model in series to the measured 1-port.

Fig. 16 shows the filter attached to the HV side of the inverter. The same is done in both 3D models. Again, after 3D computation, a 7-port network is obtained with six ports for excitation and the seventh for observation.

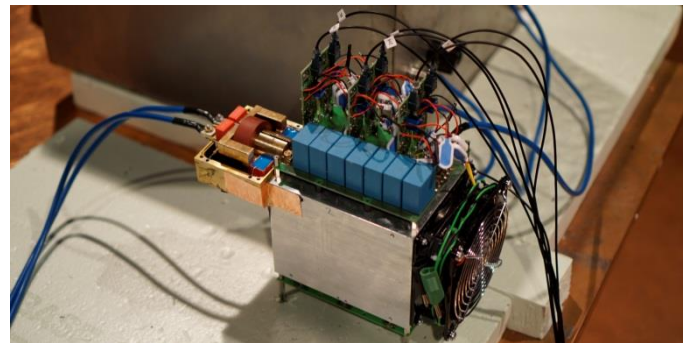


Fig. 16. Pictured of investigated filter assembled to the SiC traction inverter.

The following section uses the time domain results of Sect. III together with the different frequency domain models of Sect. IV and Sect. V to simulate the conducted and radiated emission with and without the presented filter.

## VI. SYSTEM SIMULATION RESULTS

All following measurement results are recorded with an oscilloscope and transformed into frequency domain using an FFT algorithm. For the sake of comparability an envelope function with 1000 logarithmically distributed points is applied to the spectra. Only the peak values between those points are plotted in the following results.

Fig. 17 compares the CM (common-mode) and DM (differential-mode) currents on the battery-cable in front of the LISN. In the test setup, the currents are measured with an F65 (Fischer) current clamp, in the simulation they are calculated using mode-converters in CST Design Studio.

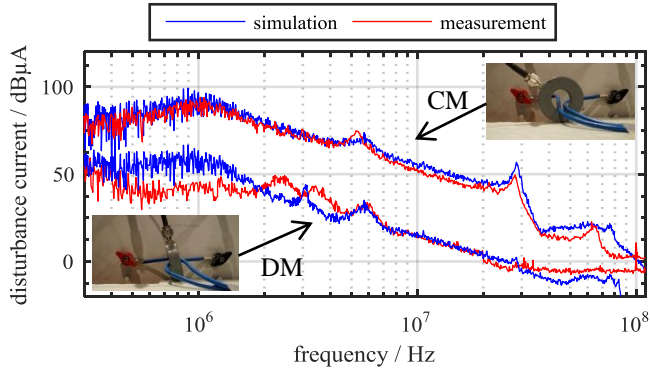


Fig. 17. Comparison between simulated and measured common- and differential mode at the battery cables in front of the LISN.

Below 40 MHz, the CM currents are reproduced precisely by the simulation with an accuracy of  $\pm 3$  dB. For higher frequencies, the deviation between both curves becomes larger caused by the transient simulation results. For DM currents the deviations are larger especially in the low frequency range. For both currents, the results can be improved if the transient transistor capacitances are considered to the MOSFET model. The estimation of these capacitances with the method presented in [7] is object of current work. The good agreement of the currents affects directly the disturbance voltage at the LISN, at the monopole antenna and at the biconical antenna. The simulation results for these voltages without the assembled filter (Fig. 18) and the results including the filter (Fig. 19) are in good accordance with the measurements of the LISN and the biconical antenna. It can be concluded that the presented approach is suited for the simulation of radiated emissions caused by traction inverters in a CISPR25 test setup. However, the deviations appearing in the DM current and the monopole voltage require further investigations.

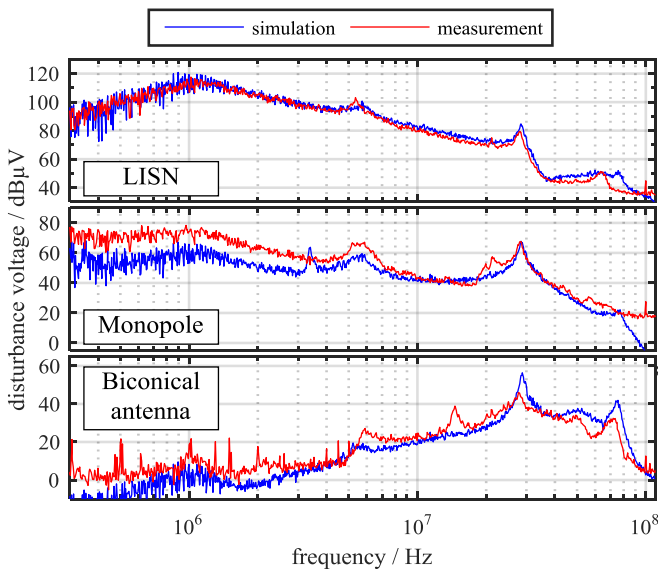


Fig. 18. Simulation result of the disturbance voltages without filter.

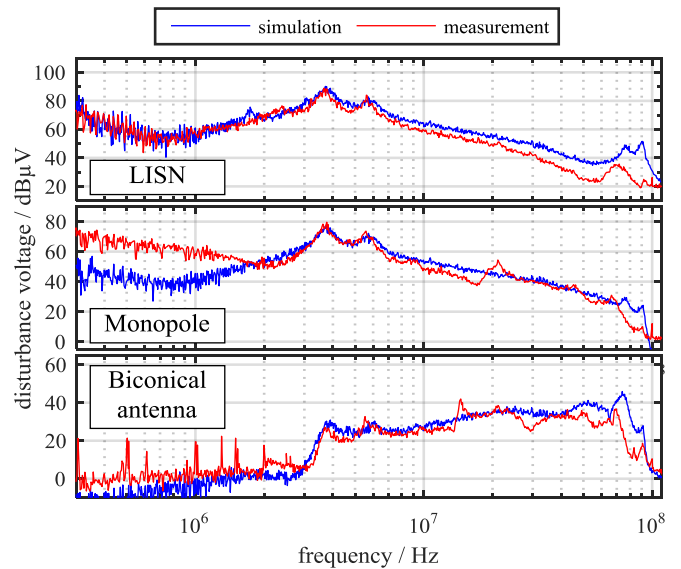


Fig. 19. Simulation result of the disturbance voltages with filter.

## VII. CONCLUSION

The paper presents a new simulation method for conducted and radiated emissions of a SiC inverter in a CISPR25 test setup. The method consists of two parts. First, a geometry model of the inverter's commutation-cell is presented which is used to derive a transient simulation of the drain-source voltages of all MOSFETs. Subsequent, the time domain results are transformed into frequency domain and combined with a frequency domain simulation based on different 3D geometry models of the complete test setup. The combination of both simulations can reproduce the emissions in the frequency range up to 110 MHz. The considerable small total simulation time of this approach enables an effective filter development.

## REFERENCES

- [1] K. Kumar, M. Bertoluzzo and G. Buja, "Impact of SiC MOSFET traction inverters on compact-class electric car range," IEEE PEDES, Mumbai, India, 2014, pp. 1-6.
- [2] L. Kotny, T. Duquesne and N. Idir, "Modeling and design of the EMI filter for DC-DC SiC-converter", International Symposium on Power Electronics, Ischia, Italy, 2014, pp. 1195-1200.
- [3] P. Hillenbrand, C. Keller, K. Spanos, S. Tenbohlen: "Understanding Conducted Emissions from an Automotive Inverter Using a Common-Mode Model", IEEE EMC Europe (Joint Co.), Dresden, Germany, 2015.
- [4] P. Hillenbrand, M. Böttcher, S. Tenbohlen and J. Hansen, "Frequency-domain EMI-simulation and resonance analysis of a DCDC-converter," EMC Europe, Wroclaw, Poland, 2016, pp. 176-181.
- [5] F. Traub, J. Hansen, W. Ackermann, Th. Weiland: "Automated construction of physical equivalent circuits for inductive components", EMC Europe, 2013, pp. 67-72.
- [6] P. Hillenbrand, M. Beltle, S. Mönch, S. Tenbohlen: "Sensitivity Analysis of Behavioral MOSFET Models in Transient EMC Simulation" in international Symposium on EMC, Anger, France, 2017.
- [7] V. Hoch, J. Petzoldt, H. Jacobs, A. Schlogl and G. Deboy, "Determination of transient transistor capacitances of high voltage MOSFETs from dynamic measurements," International Symposium on Power Semiconductor, Barcelona, Brasilia, 2009, pp. 148-151.
- [8] B. Gustavsen, A. Semlyen: "A Robust Approach for System Identification in the Frequency Domain", IEEE Trans. on Power Delivery, vol. 19, no. 3, July 2004.
- [9] A. E. Ruehli, "Equivalent circuit models for three dimensional multiconductor systems", IEEE Trans. Microw. Theory Techn., vol. 22, no. 3, Mar. 1974.